Doubly enhanced second harmonic generation through structural and epsilon-near-zero resonances in TiN nanostructures

Wen, Xinglin; Li, Guangyuan; Gu, Chengyan; Zhao, Jiaxin; Wang, Shijie; Jiang, Chunping; Palomba, Stefano; Martijn de Sterke, C.; Xiong, Qihua

2018

Wen, X., Li, G., Gu, C., Zhao, J., Wang, S., Jiang, C., . . . Xiong, Q. (2018). Doubly enhanced second harmonic generation through structural and epsilon-near-zero resonances in TiN nanostructures. ACS Photonics, 5(6), 2087-2093. doi:10.1021/acsphotonics.8b00419

https://hdl.handle.net/10356/140369

https://doi.org/10.1021/acsphotonics.8b00419

Doubly-enhanced Second Harmonic Generation through Structural and Epsilon-near-zero Resonances in TiN Nanostructures

Xinglin Wen[1,†], Guangyuan Li[2,3,†], Chengyan Gu[4], Jiaxin Zhao[1], Shijie Wang[5] Chunping Jiang[4,], Stefano Palomba[2,3,6,*], C. Martijn de Sterke[2,3], and Qihua Xiong[1,7,8,*]*

[1]Division of Physics and Applied Physics, School of Physical and Mathematical Sciences, Nanyang Technological University, Singapore 637371

[2]Institute of Photonics and Optical Science (IPOS), School of Physics, The University of Sydney, NSW, Australia 2006

[3]Centre for Ultrahigh-bandwidth Devices for Optical Systems (CUDOS), School of Physics, The University of Sydney, NSW, Australia 2006

[4]Key Laboratory of Nanodevices and Applications, Suzhou Institute of Nano-Tech and Nano-Bionics, CAS, Suzhou, China 215123

[5]Institute of Materials Research & Engineering, Agency for Science, Technologies and Research, 2 Fusionopolis Way, Singapore 138634

[6]The University of Sydney Nano Institute, The University of Sydney, NSW, Australia 2006

[7]NOVITAS, Nanoelectronics Centre of Excellence, School of Electrical and Electronic Engineering, Nanyang Technological University, Singapore 639798

[8]MajuLab, CNRS-UCA-SU-NUS-NTU International Joint Research Unit, UMI 3654 Singapore

[†]These authors contribute to this work equally

[*]To whom correspondence should be addressed. Email address: Qihua@ntu.edu.sg, cpjiang2008@sinano.ac.cn and stefano.palomba@sydney.edu.au.

Abstract

Enhancing the nonlinear frequency conversion efficiency at the nanoscale is important for on-chip communication, information processing and sensing. Plasmonic nanostructures can significantly enhance the nonlinear signal due to localized surface plasmon (LSP) resonances, *i.e.*, localized electric field enhancements. Ideally, a double resonance occurs, in which both the excitation and the harmonic wavelengths are enhanced, but this is restricted by the available modes. It has been recently shown that thin films of epsilon-near-zero (ENZ) materials can also enhance optical nonlinear effects if excited at the ENZ wavelength. Here, we report the first demonstration of a new mechanism to enhance the second harmonic generation (SHG), combining a structural LSP resonance at the fundamental frequency, and the material ENZ resonance at the second harmonic frequency. We show that when both resonances are present, the SHG is substantially enhanced. With its refractory nature and CMOS compatibility, our results show considerable promise for TiN micro and nanostructures in integrated on-chip nonlinear optical devices.

Keywords: Second harmonic generation, epsilon-near-zero (ENZ) materials, titanium nitride, magnetic resonance, doubly enhanced SHG

Introduction

Enhancing the harmonic generation conversion efficiency at the nanoscale is a critical challenge in nonlinear optics. Nonlinear nanophotonics is particularly promising, since nanoscale structures do not require phase-matching[1] due to their sub-wavelength dimensions, which further make it possible to utilize the resonant field enhancement to enhance nonlinear effects. Several systems have been proposed and reported in the literature. These include nonlinear optical signal generation from metallic nanostructures[1-4], hybrid metal-dielectric systems[5-7], resonators[8, 9] and so on. In all these platforms the electric field at either the fundamental or the harmonic wavelength is enhanced[1]. This efficiency can be further increased if the fields at both the fundamental and the harmonic wavelengths resonate simultaneously[10-12], like, for instance, in multi-resonant plasmonic nanoantennae in the work of Celebrano *et al*[10]. However, one of the two modes was an electric quadrupole mode, which exhibits low field confinement and therefore leads to modest nonlinear optical enhancement.

Recently, epsilon-near-zero (ENZ) engineered materials have attracted tremendous attention because there is no phase accumulation when light propagates through such a medium, which enables waveform tailoring[13], light tunnelling[14] and light trapping[15]. The ENZ condition can either be achieved in artificial metamaterials[16-18], or by controlling the growth conditions, in films made of materials such as indium tin oxide[19, 20 21](ITO) and titanium nitride[19] (TiN). Simulations show that the electric field can be strongly confined inside the film when the excitation wavelength matches the ENZ wavelength (termed the "ENZ mode")[22-24]. As theoretically predicted and experimentally demonstrated[23-26], the ENZ resonance in these films thus provides an alternative avenue for SHG enhancement.

Though both second-order[19] and third-order[20] nonlinearities can be enhanced in ITO films when excited at the ENZ wavelength, this resonance cannot be combined with LSP resonance enhancement because ITO has very poor plasmonic behaviour. Hence, we propose TiN as a good candidate to demonstrate a double resonance effect, where the excitation and the SHG wavelength are enhanced, respectively, by the LSP and the ENZ resonances. TiN has its ENZ wavelength in the visible (VIS), while it has pronounced plasmonic behaviour in the near-infrared (NIR)[27-29]. Consequently, a TiN nanostructure can be tailored to exhibit a plasmonic resonance in the NIR (excitation wavelength), while its ENZ wavelength simultaneously lays in the VIS (SHG wavelength), as illustrated in Fig. 1a and 1b. We note that TiN has been investigated as an alternative plasmonic material to noble metals[30-34], that provides advantages such as: tunable optical properties due to the stoichiometry[28, 33]; it is refractory with high melting point (~2900 °C)[35, 36]; exhibiting plasmonic response in visible to near-infrared regime[37]; and large second and third-order nonlinearity[19, 36, 38]. TiN plasmonic structures are therefore well-suited for nonlinear optical applications since they can sustain high-power excitation and they exhibit strong nonlinearities[36]. More importantly, the growth of TiN film is compatible with CMOS technology to make an integrated nonlinear optics system.

While TiN nanoantennae can enhance SHG via their electric resonance[36], magnetic resonance enhancement of nonlinear effects has recently attracted interest. This enhancement, which has quite different properties compared with electric dipole resonance enhancement[39-41], has been attributed to the Lorentz force acting on the oscillating electrons in the resonator[39], and has been demonstrated in metallic split ring resonators[39], metasurface[42] and a high index dielectric materials[43-45].

In this report, we first investigate the TiN split ring resonators fabricated starting from the as-grown thin film, and show that both the electric and magnetic resonances can be resolved. Secondly, we validate SHG enhancement at the ENZ wavelength in homogeneous TiN thin films. Thirdly, we investigate the ENZ and plasmonic double resonance, and show that it substantially enhances the SHG. Our results show that when the magnetic resonance of the resonators and the ENZ wavelength of the material coincide, respectively, with the excitation wavelength and the harmonic wavelength, then the strongest nonlinear signal is observed.

Results and Discussion

A 50 nm TiN thin film was grown on a sapphire substrate by pulsed laser deposition (PLD) under a nitrogen gas atmosphere (see details in methods). The crystal structure of the as-grown film was then characterized by X-ray diffraction as shown in Fig. 2a; the (111) and (222) peaks indicate that the as-grown TiN film crystallize in the cubic phase. The surface roughness is determined to be ~1.3 Å by atomic force microscopy (Fig. 2b). Electron beam lithography (EBL) was utilized to pattern a conventional negative resist - hydrogen silsesquioxane (HSQ) - coated on a TiN substrate, to fabricate TiN nanostructures. Subsequently, the HSQ pattern was transferred to TiN thin film by a reactive ion etching (RIE) process. The shape and dimensions of the resonators are defined in Fig. 2c. The typical split ring resonator array with a bar width of 30 nm (labelled as U30) in Fig. 2d (the actual area is $50 \times 50\ \mu m^2$), shows the quality and uniformity of our fabricated samples. The linear optical properties were characterized by conventional transmission measurements using a micro-spectrophotometer (CRAIC 20). When the excitation polarization is parallel to the ring gap, both an electric mode (high energy, indicated by black dashed line) and a magnetic

mode (low energy, indicated by yellow dashed line) are observed (Fig. 2e). It is well known that the electric mode arises from the electric dipole of the two vertical bar of the resonator, while the magnetic mode emerges from the circulating current along the ring[46-51]. By increasing the resonator size, both the electric and magnetic modes are red shifted. Transmission spectra, calculated with the finite-difference time-domain (FDTD) method, by using the measured dielectric constant of the TiN film, are in good agreement with the experimental measurements (Fig. 2f).

The dielectric constant of the TiN was retrieved from ellipsometry reflectance measurements by a Drude mode fit as shown in Fig. 3a. The real part of the permittivity vanishes at wavelengths around 520 nm, which corresponds to the ENZ wavelength. For wavelengths longer than 520 nm, the real part of the permittivity is negative and TiN supports plasmonic behaviour.

The SHG of the uniform TiN thin film was measured by an optical microscope in reflection mode, coupled to an imaging spectrometer and a VIS CCD camera. The results for excitation wavelengths between 850 and 1080 nm (Ti:Sapphire femtosecond laser) are shown in Fig. 3b. The average excitation power at each wavelength was kept constant at ~6 mW. Each black spectrum corresponds to the measured SHG emission at a fixed excitation wavelength. Integrating each of these curves gives the blue dots, which thus indicate the integrated SHG intensity at each wavelength. Finally, the red curve is a polynomial fit. It is evident that the SHG intensity is largest at the ENZ wavelength of 520 nm; here the SHG intensity is enhanced by about a factor of 5 compared to the SHG intensity at 425 nm. We attribute this enhancement, which is somewhat higher than that reported in the literature[19], to the ENZ resonance of the TiN film. Because no SHG signal can be detected from the sapphire substrate under the same excitation condition, we thus confirm that all the SHG signal comes from the TiN.

It is important to note that in all the reported observations of enhanced nonlinearities in ENZ materials[20, 25, 26], the excitation wavelength coincides with the ENZ wavelength and oblique incidence is required[20, 25, 26]. In contrast, here ENZ resonance coincides with the harmonic wavelength, and the SHG is emitted at an angle of ~27°, which is easily collected by our microscope objective (0.85 numerical aperture). It should further be noted that the SHG from the TiN thin film does not depend on the polarization of the excitation field.

As shown in Fig. 2e, our TiN resonators exhibit magnetic resonances in the NIR, which can be tailored by fabrication to be twice the ENZ wavelength, enabling double resonance enhancement of the SHG (see Fig. 1b). We fabricated resonator arrays with different sizes to tune the magnetic resonance. Resonators with a bar width of 20 nm (U20) exhibit a magnetic resonance at 1040 nm under parallel excitation (Fig. 2e), which is double the ENZ wavelength of the TiN (520 nm). Therefore, we expect the U20 to be the structure to show the double resonance effect.

The SHG of U20 was measured by sweeping the excitation wavelength over the magnetic resonance line shape (850-1080 nm) under parallel excitation. The resulting SHG spectra are shown in Fig. 4a (blue curves). SHG spectra were also measured under the same conditions, but with vertical polarization, as shown in Fig. 4a (magenta curves). It is evident that the SHG from the U20 nanoantennae is enhanced compared to that from the bare TiN thin film (Fig. 3b), under parallel polarization, whereas the SH enhancement under vertical polarized excitation is negligible.

Fig. 4b shows the transmission spectra (left axis) and SHG enhancement factor (right axis) in the same plot. The SHG enhancement factor is obtained by normalizing the SHG of the resonator to the SHG of TiN film at each wavelength. The upper and lower panels in Fig. 4b represent the observed SHG respectively under parallel and

vertical excitation. For parallel excitation (upper panel of Fig. 4b), the SHG enhancement (blue dots) follows the magnetic mode curve and reaches a maximum (16 times) at the magnetic resonance wavelength (1040 nm, black transmission curve). For the same structure (U20) the electric dipole resonance is at 850 nm under vertically polarized excitation (lower panel of Fig. 4b). It shows weakly enhanced SHG (2 times) since the SHG wavelength is away from the ENZ resonance. Fig. 4c compares the SHG enhancement at parallel and vertical polarization. The green area indicates the ENZ regime, and the plasmonic magnetic and electric resonances under parallel and vertical excitation are indicated respectively by black and yellow arrows. We attribute the different SHG enhancement under different polarizations to the plasmonic and ENZ resonances matching. Double excitation, where we excite the magnetic resonance at the fundamental frequency, and we also exploit the ENZ resonance at the SH, leads to strong SHG enhancement, is only achieved for parallel excitation.

Figure 5a show typical SHG signals from the sapphire substrate, the TiN thin film and the U20 resonators, with an excitation wavelength of 1020 nm under parallel excitation. It confirms the lack of SHG from the sapphire substrate, and that the SHG signal from resonator is much stronger than that of the film. The dependence of the SHG on the excitation power is shown in Fig. 5b. The fitted slope of around 2, indicates a quadratic relation. It can be seen that the actual slope (1.89) is slightly smaller than the theoretic value of 2, which was also observed in the SHG of TiN nanoantennas[36]. The polarization dependent SHG at 1020 nm excitation of U20 resonator is shown in Fig. 5c. The observed dipolar behaviour occurs because for polarization parallel to the resonator gap (0° and 180°), the magnetic resonance is coincides with the excitation wavelength and the SHG is enhanced. In contrast, under the vertical polarization (90°

and 270°), the plasmonic electric mode resonance (850 nm) is far away from the excitation wavelength and the double resonance does not occur.

Conclusion

In conclusion, high quality TiN thin film was grown by PLD and SHG enhancement of the TiN thin film was observed at the ENZ wavelength. Well-defined TiN split ring resonator arrays were fabricated by electron beam lithography. Experimental measurement and theoretical calculation of the linear property of TiN nanostructure show good plasmonic response in the visible and the near infrared spectrum region. Using these arrays we demonstrated a double resonance effect in which the SHG is enhanced simultaneously by the presence of a magnetic resonance at the excitation frequency, and an ENZ resonance at the second harmonic frequency. This represent the first demonstration of a new strategy to enhance optical nonlinearities in nanoscale size structures, which may enable the application in light source generation, material analysis and optical sensors.

Methods

TiN film growth. The TiN thin film was deposited on commercial sapphire substrate by pulsed laser deposition (PLD) method. A nominally stoichiometric polycrystalline TiN target of 99.9% purity was used and was placed parallel to the substrate at a distance of 70 mm. Before loading it into the chamber, the substrate was ultrasonically cleaned for 3 minutes in acetone, alcohol, deionized water, and then blown by pure N_2 gas. After loading the substrate into the chamber, the chamber was evacuated to 5.0×10^{-6} Pa by a turbo molecular pump. A KrF excimer laser beam (λ= 248 nm, τ= 25 ns) was focused on the rotated TiN target at an incidence angle of 45°. In order to remove the contaminated surface layer of the target, it was pre-sputtered for about 10 minutes.

During deposition, the laser beam energy was set at 350 mJ with a pulse repetition of 2 Hz. The substrate temperature was fixed at 650 °C. The deposition of the TiN thin film was carried out in high-purity nitrogen (99.999%) ambient with pressure at 1Pa.

TiN nanostructure fabrication. Negative electron beam resist hydrogen silsesquioxane (HSQ) (Dow Corning XR-1541) was spin-coated on TiN with the spin rate of 4000 RPM and then baked at 80°C for 4 minutes. We then used a scanning electron microscope (JEOL 7001F) equipped with the nanometer pattern generation system (NPGS) to pattern the HSQ. The exposed HSQ was developed in 25% TMAH for 30 seconds at 80°C and rinsed by water and dried by N_2 gas. The HSQ pattern was then transferred to TiN by a reactive ion etching (RIE) process.

Optical measurement. For the transmission measurements, we used a microspectrophotometer (Craic 20) which can measure sample as small as 10 μm. The measurement range spans from 300 to 2100 nm. SHG measurements were performed on an imaging spectrometer (Princeton Instruments model SCT-320 and Horiba-JY HR800) in a reflective configured optical microscope using femtosecond laser pulses as excitation. These 200 fs pulses were produced by a conventional Ti:Sapphire oscillator (Chameleon Ultra II of Coherent, Inc.) with wavelength range of 850-1080 nm and 80 MHz repetition rate. Before the backscattered light entering CCD, a 700 nm short-pass filter was added to eliminate the laser beam and let the SHG pass through.

Corresponding Authors

*Email: Qihua@ntu.edu.sg, cpjiang2008@sinano.ac.cn and stefano.palomba@sydney.edu.au.

Acknowledgements

Q.X. gratefully acknowledges the support from the Singapore National Research Foundation through the NRF Investigatorship Award (NRF-NRFI2015-03), and the Singapore Ministry of Education via two AcRF Tier 2 grants (MOE2015-T2-1-047 and MOE2017-T2-1-040) and Tier 1 grant (RG 113/16). C.J acknowledges the NANO-X Workstation of Chinese Academy of Sciences, Jiangsu Province, Suzhou City, Suzhou Industrial Park.

Author contributions

X.L.W, G.Y.L and Q. X. conceived the idea and designed the experiments; C.Y.G and C.P.J conducted the TiN thin film growth and x-ray diffraction characterizations; X.L.W and S.J.W fabricated the TiN nanostructure; X.L.W and G.Y.L performed the optical measurements; X.L.W, G.Y.L, S.P., C.M.D.S and Q.X analyzed the data; X.L.W, G.Y.L and Q.X. wrote the manuscript. All authors discussed and commented on the manuscript.

Notes

The authors declare no competing financial interest.

References

1. Kauranen, M.; Zayats, A. V. Nonlinear Plasmonics. *Nat. Photon.* **2012,** *6*, 737-748.
2. Zharov, A. A.; Shadrivov, I. V.; Kivshar, Y. S. Nonlinear Properties of Left-Handed Metamaterials. *Phys. Rev. Lett.* **2003,** *91*, 037401.
3. Dong, Z.; Asbahi, M.; Lin, J.; Zhu, D.; Wang, Y. M.; Hippalgaonkar, K.; Chu, H. S.; Goh, W. P.; Wang, F.; Huang, Z.; Yang, J. K. Second-Harmonic Generation from Sub-5 nm Gaps by Directed Self-Assembly of Nanoparticles onto Template-Stripped Gold Substrates. *Nano Lett.* **2015,** *15*, 5976-5981.
4. Ding, S. J.; Yang, D. J.; Liu, X. L.; Nan, F.; Cheng, Z. Q.; Im, S. J.; Zhou, L.; Wang, J. F.; Wang, Q. Q. Asymmetric Growth of Au-Core/Ag-Shell Nanorods with a Strong Octupolar Plasmon Resonance and an Efficient Second-Harmonic Generation. *Nano Res.* **2018,** *11*, 686-695.
5. Liu, X. F.; Zhang, Q.; Chong, W. K.; Yip, J. N.; Wen, X. L.; Li, Z. P.; Wei, F. X.; Yu, G. N.; Xiong, Q. H.; Sum, T. C. Cooperative Enhancement of Second-Harmonic Generation from a Single Cds Nanobelt-Hybrid Plasmonic Structure. *ACS Nano* **2015,** *9*, 5018-5026.
6. Casadei, A.; Pecora, E. F.; Trevino, J.; Forestiere, C.; Ruffer, D.; Russo-Averchi, E.; Matteini, F.; Tutuncuoglu, G.; Heiss, M.; Fontcuberta i Morral, A.; Dal Negro, L. Photonic-Plasmonic Coupling of Gaas Single Nanowires to Optical Nanoantennas. *Nano Lett.* **2014,** *14*, 2271-2278.
7. Lee, J.; Tymchenko, M.; Argyropoulos, C.; Chen, P. Y.; Lu, F.; Demmerle, F.; Boehm, G.; Amann, M. C.; Alu, A.; Belkin, M. A. Giant Nonlinear Response from Plasmonic Metasurfaces Coupled to Intersubband Transitions. *Nature* **2014,** *511*, 65-69.
8. Pu, Y.; Grange, R.; Hsieh, C. L.; Psaltis, D. Nonlinear Optical Properties of Core-Shell Nanocavities for Enhanced Second-Harmonic Generation. *Phys. Rev. Lett.* **2010,** *104*, 207402.
9. Fryett, T. K.; Seyler, K. L.; Zheng, J.; Liu, C.-H.; Xu, X.; Majumdar, A. Silicon Photonic Crystal Cavity Enhanced Second-Harmonic Generation from Monolayer WSe_2. *2D Materials* **2016,** *4*, 015031.
10. Celebrano, M.; Wu, X.; Baselli, M.; Grossmann, S.; Biagioni, P.; Locatelli, A.; De Angelis, C.; Cerullo, G.; Osellame, R.; Hecht, B.; Duo, L.; Ciccacci, F.; Finazzi, M. Mode Matching in Multiresonant Plasmonic Nanoantennas for Enhanced Second Harmonic Generation. *Nat. Nanotechnol.* **2015,** *10*, 412-417.
11. Liu, S. D.; Leong, E. S.; Li, G. C.; Hou, Y.; Deng, J.; Teng, J. H.; Ong, H. C.; Lei, D. Y. Polarization-Independent Multiple Fano Resonances in Plasmonic Nonamers for Multimode-Matching Enhanced Multiband Second-Harmonic Generation. *ACS Nano* **2016,** *10*, 1442-1453.
12. Aouani, H.; Navarro-Cia, M.; Rahmani, M.; Sidiropoulos, T. P.; Hong, M.; Oulton, R. F.; Maier, S. A. Multiresonant Broadband Optical Antennas as Efficient Tunable Nanosources of Second Harmonic Light. *Nano Lett.* **2012,** *12*, 4997-5002.
13. Alù, A.; Silveirinha, M. G.; Salandrino, A.; Engheta, N. Epsilon-near-Zero Metamaterials and Electromagnetic Sources: Tailoring the Radiation Phase Pattern. *Phys. Rev. B* **2007,** *75*, 155410.
14. Silveirinha, M.; Engheta, N. Tunneling of Electromagnetic Energy through Subwavelength Channels and Bends Using Epsilon-near-Zero Materials. *Phys. Rev. Lett.* **2006,** *97*, 157403.

15. Silveirinha, M. G. Trapping Light in Open Plasmonic Nanostructures. *Phys. Rev. A* **2014,** *89*, 023813.
16. Liberal, I.; Engheta, N. Near-Zero Refractive Index Photonics. *Nat. Photon.* **2017,** *11*, 149-158.
17. Maas, R.; Parsons, J.; Engheta, N.; Polman, A. Experimental Realization of an Epsilon-near-Zero Metamaterial at Visible Wavelengths. *Nat. Photon.* **2013,** *7*, 907-912.
18. Moitra, P.; Yang, Y.; Anderson, Z.; Kravchenko, I. I.; Briggs, D. P.; Valentine, J. Realization of an All-Dielectric Zero-Index Optical Metamaterial. *Nat. Photon.* **2013,** *7*, 791-795.
19. Capretti, A.; Wang, Y.; Engheta, N.; Dal Negro, L. Comparative Study of Second-Harmonic Generation from Epsilon-near-Zero Indium Tin Oxide and Titanium Nitride Nanolayers Excited in the near-Infrared Spectral Range. *ACS Photonics* **2015,** *2*, 1584-1591.
20. M. Zahirul Alam; Israel De Leon; Boyd, R. W. Large Optical Nonlinearity of Indium Tin Oxide in Its Epsilon-near-Zero Region. *Science* **2016,** *352*, 795-797.
21. Wang, Y.; Capretti, A.; Dal Negro, L. Wide Tuning of the Optical and Structural Properties of Alternative Plasmonic Materials. *Opt. Mater. Express* **2015,** *5*, 2415-2430.
22. Caspani, L.; Kaipurath, R. P.; Clerici, M.; Ferrera, M.; Roger, T.; Kim, J.; Kinsey, N.; Pietrzyk, M.; Di Falco, A.; Shalaev, V. M.; Boltasseva, A.; Faccio, D. Enhanced Nonlinear Refractive Index in Epsilon-near-Zero Materials. *Phys. Rev. Lett.* **2016,** *116*, 233901.
23. Vincenti, M. A.; de Ceglia, D.; Ciattoni, A.; Scalora, M. Singularity-Driven Second- and Third-Harmonic Generation at ε-near-Zero Crossing Points. *Phys. Rev. A* **2011,** *84*, 063826.
24. Campione, S.; de Ceglia, D.; Vincenti, M. A.; Scalora, M.; Capolino, F. Electric Field Enhancement in ε-near-Zero Slabs under TM-Polarized Oblique Incidence. *Phys. Rev. B* **2013,** *87*, 035120.
25. Luk, T. S.; de Ceglia, D.; Liu, S.; Keeler, G. A.; Prasankumar, R. P.; Vincenti, M. A.; Scalora, M.; Sinclair, M. B.; Campione, S. Enhanced Third Harmonic Generation from the Epsilon-near-Zero Modes of Ultrathin Films. *Appl. Phys. Lett.* **2015,** *106*, 151103.
26. Kamandi, M.; Guclu, C.; Luk, T. S.; Wang, G. T.; Capolino, F. Giant Field Enhancement in Longitudinal Epsilon-near-Zero Films. *Phys. Rev. B* **2017,** *95*, 161105(R).
27. Boltasseva, A.; Atwater, H. A. Materials Science. Low-Loss Plasmonic Metamaterials. *Science* **2011,** *331*, 290-291.
28. Guler, U.; Ndukaife, J. C.; Naik, G. V.; Nnanna, A. G.; Kildishev, A. V.; Shalaev, V. M.; Boltasseva, A. Local Heating with Lithographically Fabricated Plasmonic Titanium Nitride Nanoparticles. *Nano Lett.* **2013,** *13*, 6078-6083.
29. Naik, G. V.; Saha, B.; Liu, J.; Saber, S. M.; Stach, E. A.; Irudayaraj, J. M.; Sands, T. D.; Shalaev, V. M.; Boltasseva, A. Epitaxial Superlattices with Titanium Nitride as a Plasmonic Component for Optical Hyperbolic Metamaterials. *Proc. Natl. Acad. Sci.* **2014,** *111*, 7546-7551.
30. Hu, J.; Ren, X.; Reed, A. N.; Reese, T.; Rhee, D.; Howe, B.; Lauhon, L. J.; Urbas, A. M.; Odom, T. W. Evolutionary Design and Prototyping of Single Crystalline Titanium Nitride Lattice Optics. *ACS Photonics* **2017,** *4*, 606-612.

31. Kamakura, R.; Murai, S.; Ishii, S.; Nagao, T.; Fujita, K.; Tanaka, K. Plasmonic–Photonic Hybrid Modes Excited on a Titanium Nitride Nanoparticle Array in the Visible Region. *ACS Photonics* **2017,** *4*, 815-822.
32. Guler, U.; Naik, G. V.; Boltasseva, A.; Shalaev, V. M.; Kildishev, A. V. Performance Analysis of Nitride Alternative Plasmonic Materials for Localized Surface Plasmon Applications. *Appl. Phys. B* **2012,** *107*, 285-291.
33. Cortie, M. B.; Giddings, J.; Dowd, A. Optical Properties and Plasmon Resonances of Titanium Nitride Nanostructures. *Nanotechnology* **2010,** *21*, 115201.
34. Guler, U.; Boltasseva, A.; Shalaev, V. M. Applied Physics. Refractory Plasmonics. *Science* **2014,** *344*, 263-264.
35. Li, W.; Guler, U.; Kinsey, N.; Naik, G. V.; Boltasseva, A.; Guan, J.; Shalaev, V. M.; Kildishev, A. V. Refractory Plasmonics with Titanium Nitride: Broadband Metamaterial Absorber. *Adv. Mater.* **2014,** *26*, 7959-7965.
36. Gui, L.; Bagheri, S.; Strohfeldt, N.; Hentschel, M.; Zgrabik, C. M.; Metzger, B.; Linnenbank, H.; Hu, E. L.; Giessen, H. Nonlinear Refractory Plasmonics with Titanium Nitride Nanoantennas. *Nano Lett.* **2016,** *16*, 5708-5713.
37. Naik, G. V.; Shalaev, V. M.; Boltasseva, A. Alternative Plasmonic Materials: Beyond Gold and Silver. *Adv. Mater.* **2013,** *25*, 3264-3294.
38. Kharintsev, S. S.; Kharitonov, A. V.; Saikin, S. K.; Alekseev, A. M.; Kazarian, S. G. Nonlinear Raman Effects Enhanced by Surface Plasmon Excitation in Planar Refractory Nanoantennas. *Nano Lett.* **2017,** *17*, 5533-5539.
39. Klein, M. W.; Enkrich, C.; Wegener, M.; Linden, S. Second-Harmonic Generation from Magnetic Metamaterials. *Science* **2006,** *313*, 502-504.
40. Linden, S.; Niesler, F. B.; Forstner, J.; Grynko, Y.; Meier, T.; Wegener, M. Collective Effects in Second-Harmonic Generation from Split-Ring-Resonator Arrays. *Phys. Rev. Lett.* **2012,** *109*, 015502.
41. Rose, A.; Huang, D.; Smith, D. R. Nonlinear Interference and Unidirectional Wave Mixing in Metamaterials. *Phys. Rev. Lett.* **2013,** *110*, 063901.
42. Kruk, S.; Weismann, M.; Bykov, A. Y.; Mamonov, E. A.; Kolmychek, I. A.; Murzina, T.; Panoiu, N. C.; Neshev, D. N.; Kivshar, Y. S. Enhanced Magnetic Second-Harmonic Generation from Resonant Metasurfaces. *ACS Photonics* **2015,** *2*, 1007-1012.
43. Kruk, S. S.; Camacho-Morales, R.; Xu, L.; Rahmani, M.; Smirnova, D. A.; Wang, L.; Tan, H. H.; Jagadish, C.; Neshev, D. N.; Kivshar, Y. S. Nonlinear Optical Magnetism Revealed by Second-Harmonic Generation in Nanoantennas. *Nano Lett.* **2017,** *17*, 3914-3918.
44. Makarov, S. V.; Petrov, M. I.; Zywietz, U.; Milichko, V.; Zuev, D.; Lopanitsyna, N.; Kuksin, A.; Mukhin, I.; Zograf, G.; Ubyivovk, E.; Smirnova, D. A.; Starikov, S.; Chichkov, B. N.; Kivshar, Y. S. Efficient Second-Harmonic Generation in Nanocrystalline Silicon Nanoparticles. *Nano Lett.* **2017,** *17*, 3047-3053.
45. Shcherbakov, M. R.; Neshev, D. N.; Hopkins, B.; Shorokhov, A. S.; Staude, I.; Melik-Gaykazyan, E. V.; Decker, M.; Ezhov, A. A.; Miroshnichenko, A. E.; Brener, I.; Fedyanin, A. A.; Kivshar, Y. S. Enhanced Third-Harmonic Generation in Silicon Nanoparticles Driven by Magnetic Response. *Nano Lett.* **2014,** *14*, 6488-6492.
46. Xu, X. L.; Peng, B.; Li, D. H.; Zhang, J.; Wong, L. M.; Zhang, Q.; Wang, S. J.; Xiong, Q. H. Flexible Visible-Infrared Metamaterials and Their Applications in Highly Sensitive Chemical and Biological Sensing. *Nano Lett.* **2011,** *11*, 3232-3238.

47. Wen, X. L.; Li, G. Y.; Zhang, J.; Zhang, Q.; Peng, B.; Wong, L. M.; Wang, S. J.; Xiong, Q. H. Transparent Free-Standing Metamaterials and Their Applications in Surface-Enhanced Raman Scattering. *Nanoscale* **2014,** *6*, 132-139.
48. Zhang, J.; Cao, C.; Xu, X. L.; Liow, C.; Li, S. Z.; Tan, P. H.; Xiong, Q. H. Tailoring Alphabetical Metamaterials in Optical Frequency: Plasmonic Coupling, Dispersion, and Sensing. *ACS Nano* **2014,** *8*, 3796-3806.
49. Wen, X. L.; Zhang, Q.; Chai, J. W.; Wong, L. M.; Wang, S. J.; Xiong, Q. H. Near-Infrared Active Metamaterials and Their Applications in Tunable Surface-Enhanced Raman Scattering. *Opt. Express* **2014,** *22*, 2989-2995.
50. Zhang, Q.; Wen, X. L.; Li, G. Y.; Ruan, Q. F.; Wang, J. F.; Xiong, Q. H. Multiple Magnetic Mode-Based Fano Resonance in Split-Ring Resonator/Disk Nanocavities. *ACS Nano* **2013,** *7*, 11071-11078.
51. Cao, C.; Zhang, J.; Wen, X. L.; Dodson, S. L.; Dao, N. T.; Wong, L. M.; Wang, S. J.; Li, S. Z.; Phan, A. T.; Xiong, Q. H. Metamaterials-Based Label-Free Nanosensor for Conformation and Affinity Biosensing. *ACS Nano* **2013,** *7*, 7583-7591.

Figures and captions

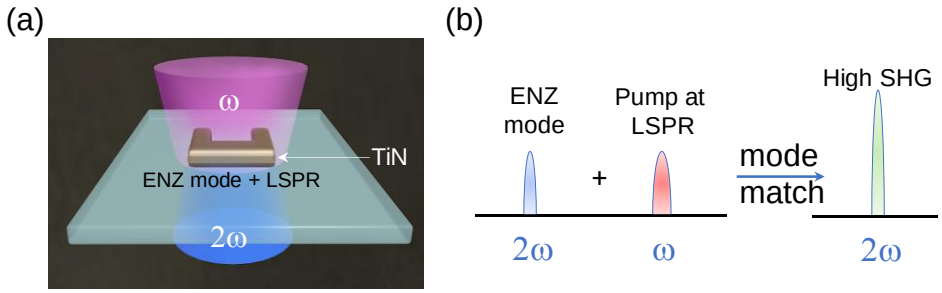

Figure 1. Principle of double resonance enhanced SHG in TiN resonators. (a) Schematic of SHG in TiN resonators, which exhibit LSPR and an ENZ mode. (b) Illustration of the mode matching: when the LSPR at the excitation wavelength matches the ENZ resonance at SH, the SHG is enhanced strongly.

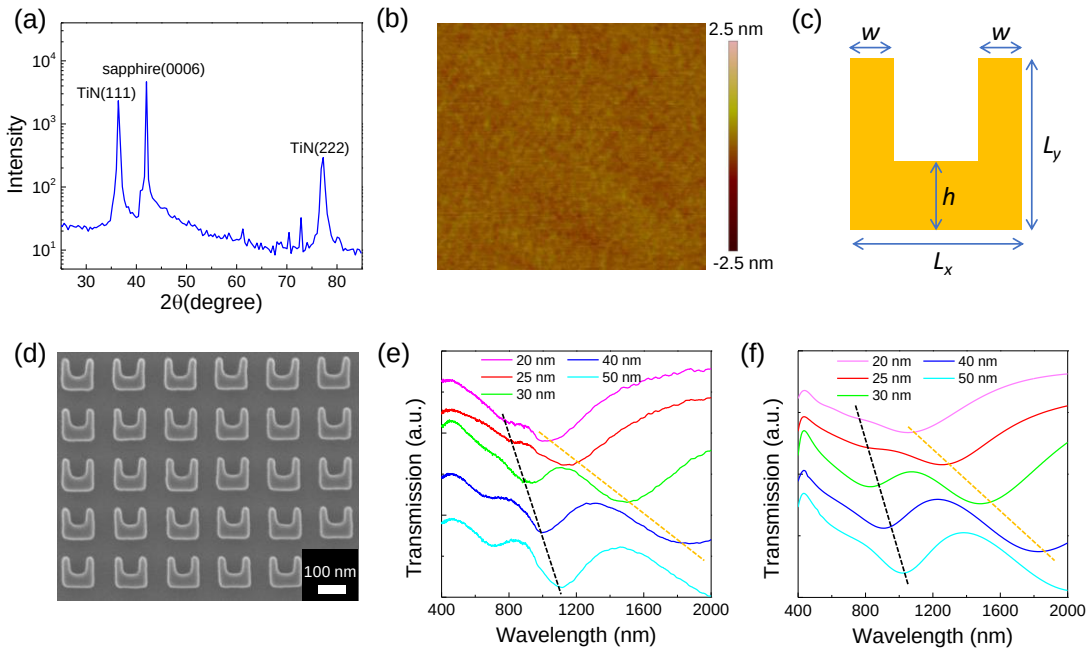

Figure 2. Linear optical properties of TiN resonators. (a) XRD of grown TiN film. (b) Roughness of the TiN surface measured by AFM. (c) Dimension of the resonator. w is the bar width, L_x=L_y=4w, h=1.6w. (d) SEM image of TiN split ring resonators with a bar width of 30 nm. (e) Measured transmission of split ring resonators with increasing bar width, showing both electric and magnetic modes. Red-shift trends are indicated by black and yellow dashed line, respectively. (f) Calculated transmission of the same structures as in (e).

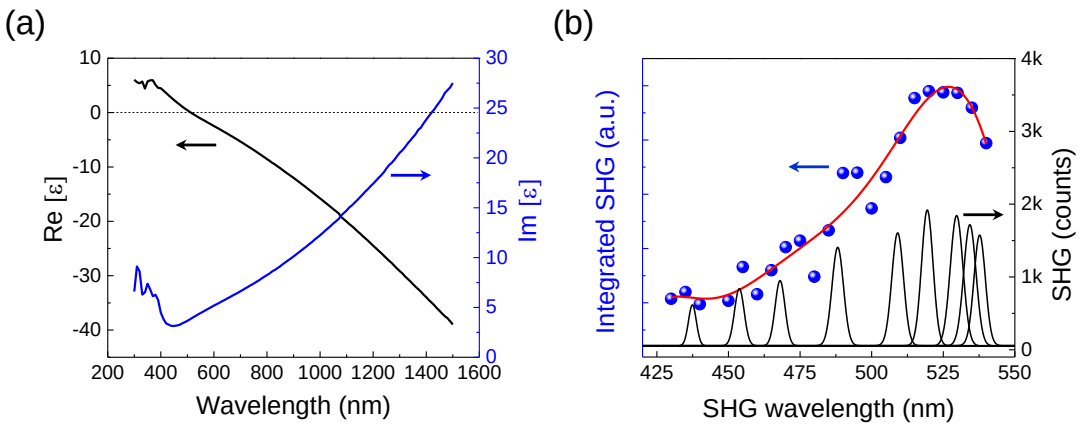

Figure 3. Epsilon-near-zero (ENZ) phenomenon and ENZ enhanced SHG in TiN film. (a) Ellipsometric permittivity of TiN film. The real part (black curve) is near zero at wavelengths around 520 nm. (b) Black curves: typical SH spectra of the TiN film for different excitation wavelengths (right axis). Blue dots: the integrated SHG spectra (left axis). Red curve: fit of the blue dots.

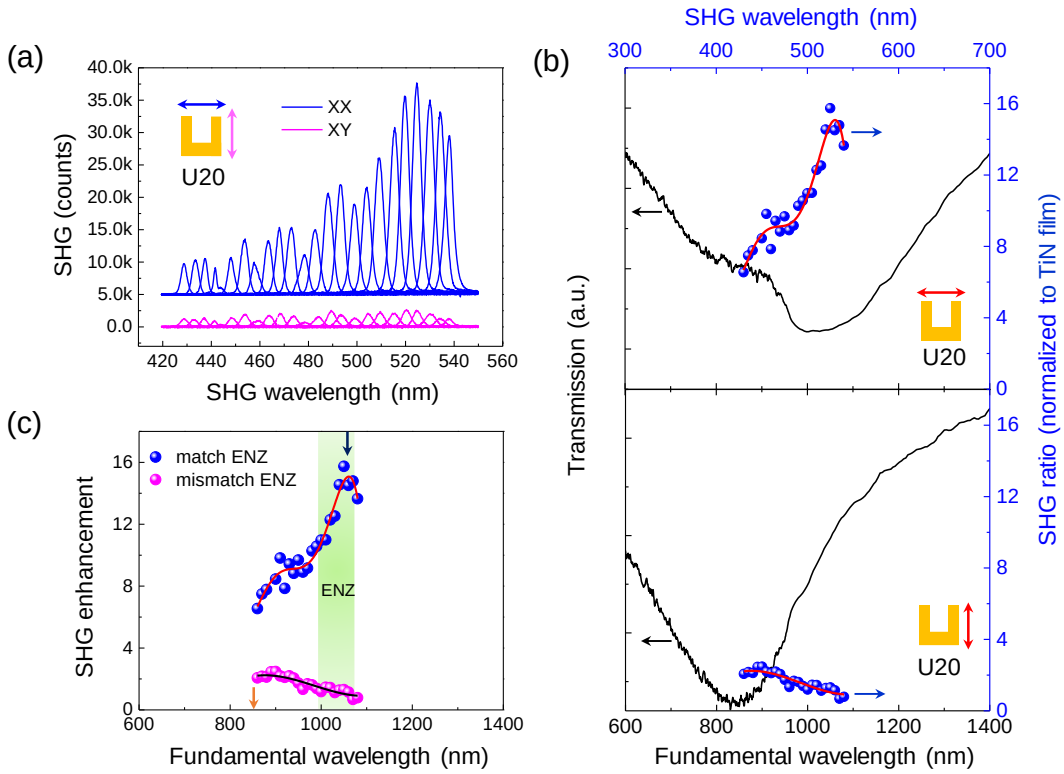

Figure 4. Double resonance enhanced SHG by matching ENZ and magnetic modes in U20 resonators. (a) Measured SHG under parallel (blue) and vertical (magenta) polarization. The former were vertically shifted for clarity. (b) Upper panel. Blue dots: normalized SHG for parallel excitation. The red curve is a fit. Black curve: linear transmission. Lower panel: same as upper panel, but for vertical polarization. (c) Extracted SHG enhancement of the two different polarizations from (b), blue and magenta dots refer to parallel and vertical polarization, respectively. Green area indicates the ENZ region. Black and yellow arrows indicate the magnetic and electric mode resonant wavelengths under parallel and vertical excitation, respectively.

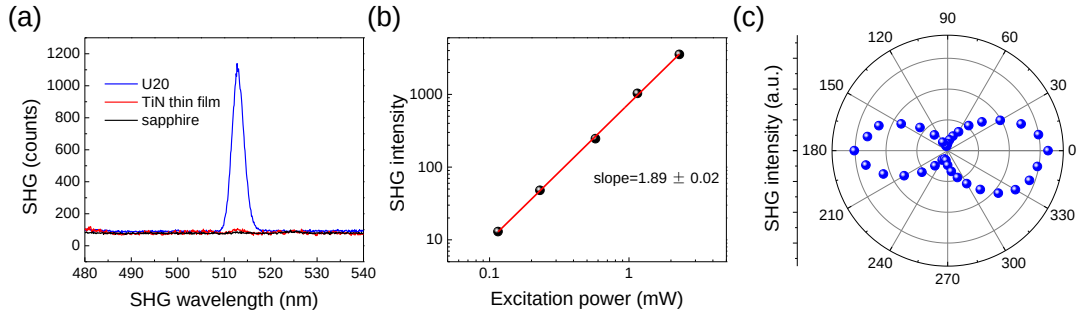

Figure 5. Additional details of the measurements (a) Comparison of the SHG of the sapphire substrate (black curve), the uniform TiN film (red curve), and double resonance (ENZ + magnetic resonance) enhanced SHG of TiN U20 resonators. (b) Power-dependent SHG of U20 resonator at 1020 nm under parallel excitation (upper case in Fig. 4b). (c) Polarization-dependent SHG of U20 resonator when pumped at 1020 nm.

TOC graphic

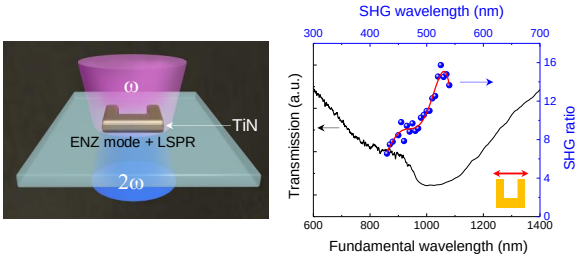
ω
TiN
ENZ mode + LSPR
2ω
SHG wavelength (nm)
300
400
500
600
700
Transmission (a.u.)
SHG ratio
0
4
8
12
16
600
800
1000
1200
1400
Fundamental wavelength (nm)